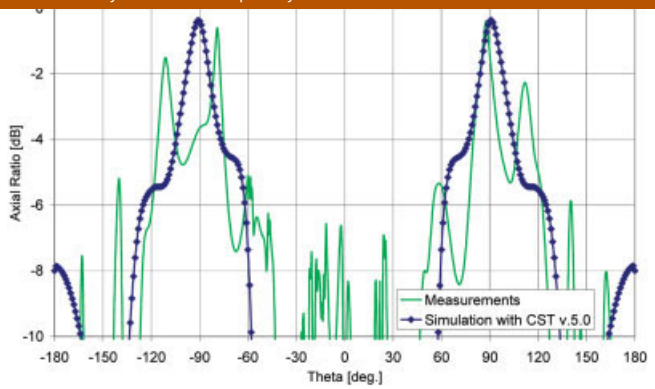

Figure 8 Axial ratio in the elevation plane. [Color figure can be viewed in the online issue, which is available at www.interscience.wiley.com]

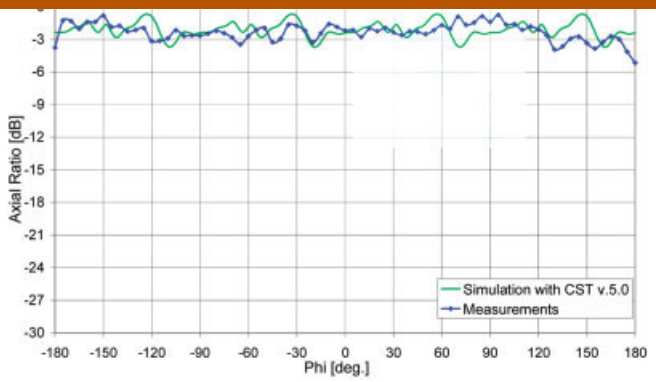

Figure 10 Axial ratio in the azimuthal plane. [Color figure can be viewed in the online issue, which is available at www.interscience.wiley.com]

5. CONCLUSION

In this study, a circularly polarized omnidirectional millimeter wave antenna for a detection of arrival signals direction system is presented. The antenna consists of a vertical conical skirt monopole and two sheets of four rows of +45° tilted parasitic strips and a foam spacer of λ/4 between the two sheets.

The simulation and experimental results show reasonable agreement. A low ripple omnidirectional radiation pattern in the azimuthal plane is achieved due to the parasitic strip elements. The manufactured prototype antenna shows successful result in circular polarization purity with this polarizer. The behavior in the extreme of the frequency band is the same as that in the central frequency.

The simple structures of the antenna, as well as the robust and simple manufacturing process, recommend the use of this antenna in the signal detection system.

ACKNOWLEDGMENTS

The simulations presented in this study have been realized using CST Microwave Studio version 5.0 under a co-operation agreement between Computer Simulation Technology (CST) and Universidad Politécnica de Madrid. This work has been developed with the support of INDRA S.A.

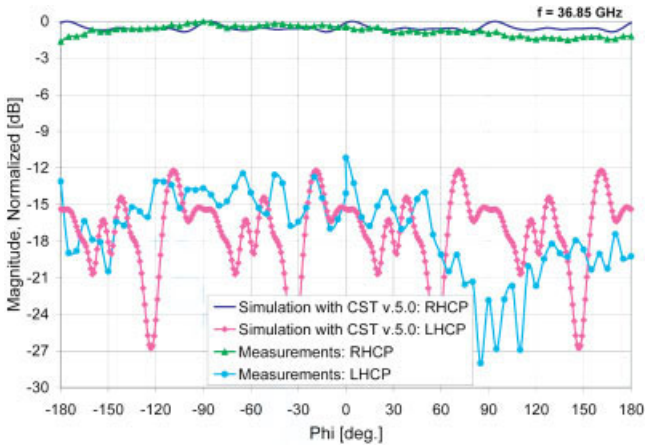

Figure 9 Compared simulated and measured radiation pattern in the azimuthal plane. [Color figure can be viewed in the online issue, which is available at www.interscience.wiley.com]

REFERENCES

1. G.H. Brown and O.M. Woodward, Circularly polarized omnidirectional antenna, RCA Rev 8 (1947), 259–269.
2. K. Sakaguchi and N. Hasebe, A circularly polarized omnidirectional antenna, In: Proceedings of the Eighth International Conference on Antennas and Propagation, Heriot-Watt University, Edinburgh, UK, March 30–April 2, 1993, Vol. 1, pp. 447–480.
3. R.S. Elliott, Antenna theory and design, Prentice-Hall, Englewood Cliffs, NJ, 1981, Section 1.18, pp. 53–56.
4. D.S. Lerner, A wave polarization converter for circular polarization, IEEE Trans Antennas Propag AP-13 (January 1965), 3–7.
5. C.A. Balanis, Antenna theory, analysis and design, Wiley, New York, 1997, Chapter 9.6, pp. 462–464.
6. J.M. Fernández and M. Sierra-Pérez, A circularly polarized omnidirectional millimeter wave antenna, Presented at the Joint COST 284 URSI Meeting, Proceedings of the 6th COST 284, Session 6C, Barcelona, Spain, September 8–10, 2004.
7. L. Young, L.A. Robinson, and C.A. Hacking, Meander-line polarizer, IEEE Trans Antennas Propagat AP-21 (May 1973), 376–378.
8. R.S. Chu and K.M. Lee, Analytical model of a multilayered meander-line polarizer plate with normal and oblique plane-wave incidence, IEEE Trans Antennas Propagat AP-35 (June 1987), 652–661.

MINIATURIZED OPTICAL FIBER BRAGG GRATING SENSOR INTERROGATOR BASED ON ECHELLE DIFFRACTIVE GRATINGS

Gaozhi Xiao,[1] Fengguo Sun,[1] Zhiyi Zhang,[1] Zhenguo Lu,[1] Jiaren Liu,[1] Fang Wu,[2] Nezih Mrad,[3] and Jacques Albert[4]
[1] Photonic Systems Group, Institute for Microstructural Science, National Research Council, M-50, 1200 Montréal Road, Ottawa, ON K1A 0R6, Canada
[2] MetroPhotonics Inc., Ottawa, ON K1C 7J2, Canada
[3] Air Vehicles Research Section, Defence R&D Canada, Department of National Defence, National Defence Headquarters, Ottawa, ON K1A 0R6, Canada
[4] Department of Electronics, Carleton University, 1125 Colonel By Drive, Ottawa, ON K1S 5B6, Canada

Received 27 July 2006

ABSTRACT: *An Optical fiber Bragg grating sensor interrogation device based on monolithically integrated echelle diffractive grating and detector arrays on an InP chip is designed and prototyped. The device*

weighs less than 60 g and measures smaller than 45 mm × 30 mm × 15 mm, and it is specifically designed for potential integration into aerospace applications. This study discusses this device's operation principle and presents some initial experimental results reflecting its performance. © 2007 Wiley Periodicals, Inc. Microwave Opt Technol Lett 49: 668–671, 2007; Published online in Wiley InterScience (www.interscience.wiley.com). DOI 10.1002/mop.22236

Key words: *fiber Bragg grating sensors; sensor interrogation; echelle diffractive gratings*

1. INTRODUCTION

Fiber Bragg grating (FBG) sensors are passive and immune to electromagnetic and radio frequency interferences. They are also light weight, small, and have very good long-term reliability. Because of the high bandwidth of optical fibers, it is possible to multiplex hundreds to thousands of FBG sensors on a single fiber strand and perform remote and distributed sensing. Within the aerospace communities, significant efforts have been devoted to embed FBG sensors into aerospace structures for the purpose of in-situ structural health monitoring [1–4]. Most of those efforts, however, have been exploratory in nature and carried out in the lab environment. This is due to the stringent requirements imposed by the industry and the lack of suitable light weight and compact size interrogators for highly multiplexed distributed or networked FBG sensors. A specific example reflecting the need of a lightweight, compact interrogator for tactical missile applications is shown in Ref. 5.

The goal of this work is to develop a miniaturized, lightweight, high resolution, solid state FBG sensor interrogator device meeting the requirements posed by the aerospace community. The approach we have taken is to use a planar lightwave circuit as the basis for this interrogator development. In this study, we report on our development and prototyping of a miniaturized fiber Bragg grating sensor interrogator device based on a monolithically integrated echelle diffractive grating (EDG) demultiplexer and photodetector arrays on an InP chip. We also discuss the operation principle of this device and report on some initial experimental results illustrating the performance of this miniaturized interrogator device.

2. OPERATION PRINCIPLE

Figure 1 shows the spectra of three multiplexed FBG sensors in a sensor network. Each of those networked FBG spectra can be described mathematically as a Gaussian distribution, i.e.

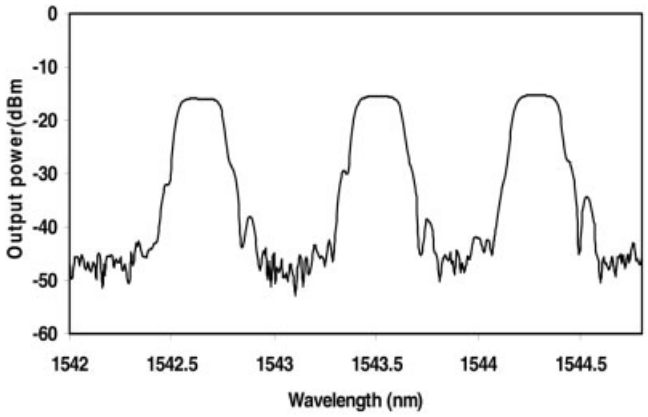

Figure 1 Example of experimentally measured reflection spectra of three FBG sensors

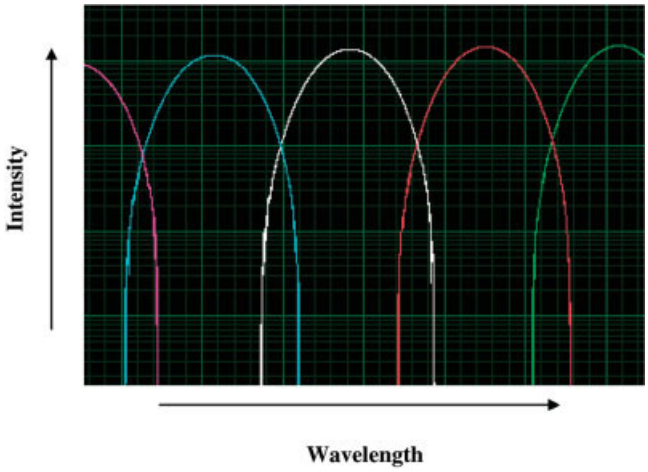

Figure 2 Illustration of the transmission spectra of a Gaussian EDG demultiplexer. [Color figure can be viewed in the online issue, which is available at www.interscience.wiley.com]

$$I_{S_i}(\lambda) = S_i \exp\left[-4(\ln 2)\frac{(\lambda - \lambda_{S_i})^2}{\Delta\lambda_{S_i}^2}\right] \quad (1)$$

where S_i, λ_{S_i}, and $\Delta\lambda_{S_i}$ are the peak transmittance, center wavelength, and full width at half maximum (FWHM) of the Gaussian profile of the i^{th} sensor in an arrayed sensor network, respectively. The error caused by this approximation is quite small and can be neglected according to the analyses given by Ref. 6. The Bragg wavelength, known as center wavelength and shown in Eq. (1), shifts in function of changes experienced in the parameters being monitored for each FBG sensor. Therefore, the key to interrogate a FBG sensor is to monitor this Bragg wavelength shift.

EDG demultiplexer is a type of demultiplexer based on planar optical waveguides [7]. These demultiplexers are initially developed for telecommunication applications. Their reliability has been proved by their deployment in optical networks. The transmission spectra of EDG demultiplexer can be designed as Gaussians, as illustrated in Figure 2, and can be expressed as

$$I_{E_j}(\lambda) = E_j \exp\left[-4(\ln 2)\frac{(\lambda - \lambda_{E_j})^2}{\Delta\lambda_{E_j}^2}\right] \quad (2)$$

where E_j, λ_{E_j}, and $\Delta\lambda_{E_j}$ are the peak transmittance, center wavelength, and FWHM of the Gaussian profile of the j^{th} channel of the EDG, respectively.

Similar to those matching principles discussed in the literature [6, 8, 9], if the j^{th} channel of the EDG can be matched to that of the i^{th} FBG sensor, the Bragg wavelengths of the sensors can be determined using the EDG demultiplexer. Figure 3 shows a set-up for the demonstration of the proposed concept. This set-up includes a broadband light source, an optical circulator, an echelle diffractive grating (EDG) demultiplexer, photodetector arrays, an electronic controller, and an array of FBGs.

It is assumed that the signal collected by the j^{th} EDG channel is mainly from the i^{th} FBG sensor, while the contribution from other FBG sensors is very small and can be neglected. This assumption can be easily satisfied by proper design of the sensor's working wavelength range. Hence, the power detected by the j^{th} EDG channel can be described by Refs. 6, 9, and 10:

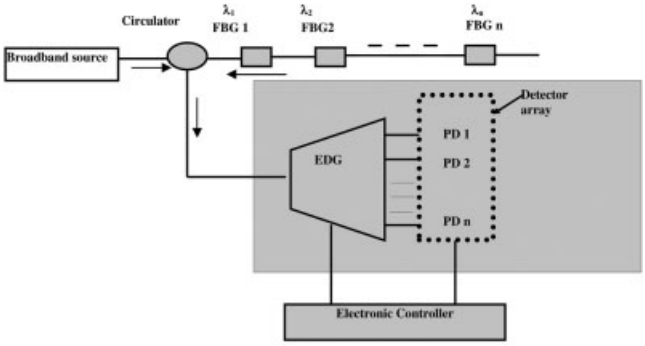

Figure 3 Illustration of the set-up for the demonstration of the operation principle of the proposed interrogator

$$I_{ji}(\lambda_{E_j}) \approx k_j E_j S_i \Delta\lambda_{E_j} \Delta\lambda_{S_i} \times \sqrt{\frac{\pi}{(\Delta\lambda_{E_j}^2 + \Delta\lambda_{S_i}^2) 4 \ln 2}} \times \exp\left[-4(\ln 2)\frac{(\lambda_{E_j} - \lambda_{S_i})^2}{\Delta\lambda_{E_j}^2 + \Delta\lambda_{S_i}^2}\right] \quad (3)$$

where k_j is a constant related to the power source and detector sensitivity. From Eq. (3) we know that the $I_{ji}(\lambda_{E_j}) - \lambda_{E_j}$ curve is a Gaussian curve with the FWHM of $\sqrt{(\Delta\lambda_{E_j}^2 + \Delta\lambda_{S_i}^2)}$ and peak value of K_j achieved when $\lambda_{E_j} = \lambda_{S_i}$ and expressed as

$$K_j = k_j E_j S_i \Delta\lambda_{E_j} \Delta\lambda_{S_i} \times \sqrt{\frac{\pi}{(\Delta\lambda_{E_j}^2 + \Delta\lambda_{S_i}^2) 4 \ln 2}} \quad (4)$$

Since the transmission wavelengths of the EDG demultiplexer change linearly with the EDG chip temperature, as shown in Figure 4, we have

$$\lambda_{E_j}(T) = BT + C \quad (5)$$

where B and C are constants and T is the EDG chip temperature. Combining Eqs. (3)–(5), we obtain

$$I_{ji}(T) = K_j \exp\left[-4(\ln 2)\frac{(BT + C - \lambda_{S_i})^2}{\Delta\lambda_{E_j}^2 + \Delta\lambda_{S_i}^2}\right] \quad (6)$$

Equation (6) shows that $I_{ji}(T)$–T curve is also a Gaussian curve with FWHM equal to $\sqrt{(\Delta\lambda_{E_j}^2 + \Delta\lambda_{S_i}^2)}$ and peak value equal to K_j. The peak value is reached when $\lambda_{S_i} = BT + C$. Hence, by finding the value

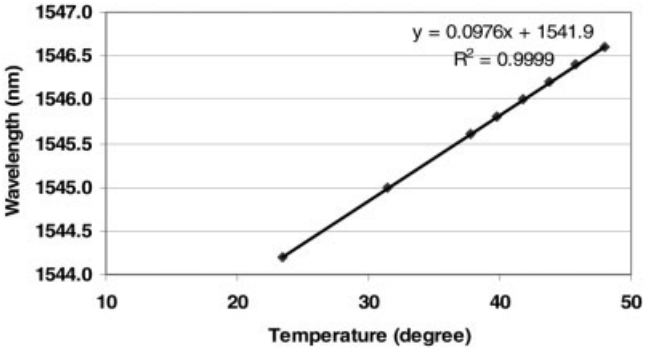

Figure 4 Example of the changes of the transmission wavelength of the EDG demultiplexer with the chip temperature (Channel 19)

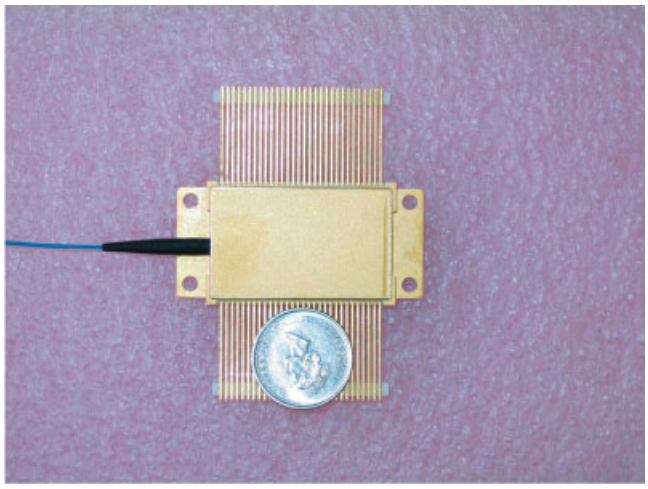

Figure 5 Illustration of a packaged miniaturized interrogator prototype. [Color figure can be viewed in the online issue, which is available at www.interscience.wiley.com]

of the EDG chip temperature corresponding to the peak of the $I_{ji}(T)$–T curve, the sensor wavelength λ_{S_i} can be determined.

3. EXPERIMENTAL RESULTS

The EDG demultiplexer and the detector arrays can be monolithically integrated on an InP chip [11]. Based on this chip, we developed a compact and lightweight interrogator prototype device. Figure 5 shows a picture of this device that weighs 60 g and has dimensions of $45 \times 30 \times 15$ mm^3. It includes a monolithically integrated EDG demultiplexer and waveguide PIN detector arrays on an InP chip, a thermoelectric cooler (TEC), a RTD sensor, and a heater dissipater. The TEC and RTD sensors were integrated with the chip for the purpose of adjusting and monitoring the temperature in the chip.

This miniaturized interrogator was used to monitor the wavelength of five arrayed and distributed fiber Bragg gratings. Figure 6 shows the response of one of the EDG channel. The results show

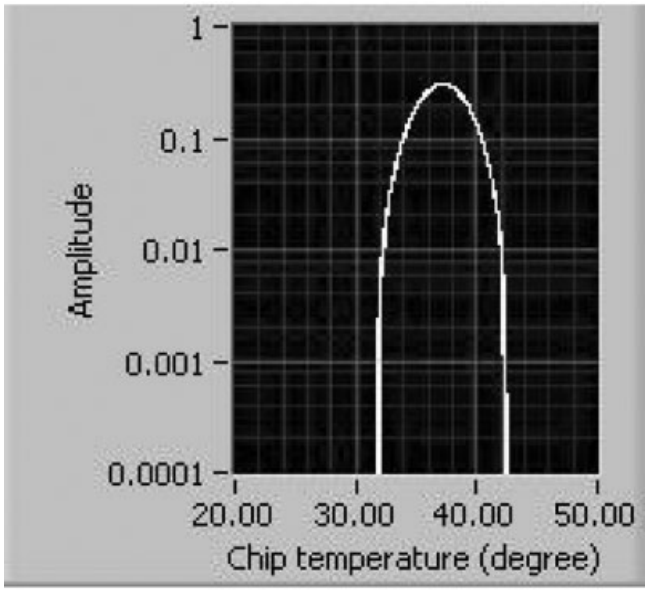

Figure 6 Example of the changes of sensor signals with the EDG chip temperature

TABLE 1 Comparison Between the Bragg Wavelengths of the FBG Sensors Measured by the Miniaturized Interrogator Prototype and Those Supplied by the Manufacturer

Sensors	Sensor Wavelength (nm)	Sensor Wavelength Supplied by the Manufacturer (nm)
1	1543.486	1543.52
2	1544.267	1544.30
3	1545.048	1545.06
4	1545.911	1545.90
5	1546.658	1546.66

a Gaussian relationship between the signal intensity and the EDG chip temperature, thus confirming Eq. (6). The measured wavelength values for the five gratings are listed in Table 1 and compared to those provided by the manufacturer. It is noted that the measurement resolution of the interrogator is better than 1 pm as the reading resolution of the EDG chip temperature is better than 0.01°C. It is further observed that the measured wavelengths are in good agreement with those provided by the manufacturer. The small variations in wavelengths can be attributed to environmental disturbances, such as the impact of temperature and strain on the grating. It is well known that Bragg wavelength shifts with temperature at a rate of ~13 pm/°C and strain at a rate of ~1.2 pm/$\mu\varepsilon$ for Bragg wavelength of 1550 nm [12].

The developed interrogator was also used to monitor temperatures. Figure 7 shows the experimental results of such temperature variation and illustrates the performance of the interrogator for temperature measurement. By monitoring the EDG temperature corresponding to the maximum optical power in a dedicated channel (Channel 19 in this case), the FBG temperature sensor can be precisely interrogated.

Through proper design of the EDG and use of current technology, 100 channels or more can be interrogated. Moreover, because of the compactness and light-weight of the interrogator, it is possible to stack several miniaturized interrogators together and increase the interrogator capability beyond the developed device presented here. Thus providing added flexibility and increasing the interrogation capability. We are currently working on employing this technology in an aerospace environment. This device is seen of significant potential in robotics, smart clothing, and security systems application requiring light-weight and compactness.

4. CONCLUSIONS

A miniaturized fiber Bragg grating sensor interrogation device based on integrated EDG has been proposed, developed, and prototyped. Results, employing this device, illustrated its performance for temperature measurement and for FBG sensor Bragg wavelength identification. This device is also able to monitor multiFBG sensors simultaneously with a resolution better than 1 pm.

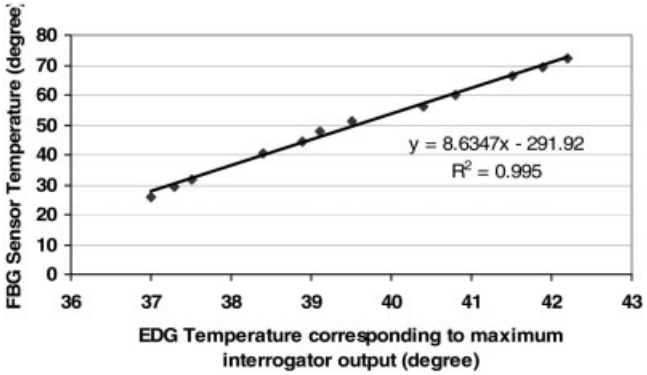

Figure 7 Interrogation result of a FBG temperature sensor using the miniaturized interrogator prototype

REFERENCES

1. J.-R. Lee, C.-Y. Ryu, B.Y. Koo, S.-F. Kang, C.-S. Hong, and C.-Gon Kim, In-flight health monitoring of a subscale wing using a fiber Bragg grating sensor system, Smart Mater Struct 12 (2003), 147–155.
2. K. Wood, T. Brown, R. Rogowski, and B. Jensen, Fiber optic sensors for health monitoring of morphing airframes. I. Bragg gating strain and temperature sensor, Smart Mater Struct 9 (2000), 163–169.
3. S.C. Galea, N. Rajic, I.G. Powlesland, S. Moss, M.J. Konak, S. Van der Velden, A.A. Baker, A.R. Wilson, S.K. Burke, I. McKenzie, Y.L. Koh, and W.K. Chiu, Overview of DSTO smart structures activities related to structural health monitoring, HUMS 2001-DSTO International Conference on Health and Usage Monitoring, Melbourne, February 19–20, 2001.
4. N. Mrad and G.Z. Xiao, Multiplexed fibre Bragg gratings for potential aerospace applications, The 2005 International Conference on MEMS, NANO, and Smart Systems, Banff, Alberta, Canada, July 24–27, 2005. pp. 359–363.
5. http://www.dodsbir.net/sitis/archives_display_topic.asp?Bookmark=27930.
6. A.B.L. Ribeiro, L.A. Ferreira, J.L. Santos, and D.A. Jackson, Analysis of the reflective-matched fiber Bragg grating sensing interrogation scheme, Appl Opt 36 (1997), 934–939.
7. J.J. He, B. Lamontagne, A. Delage, L. Erickson, M. Davies, and E.S. Koteles, Monolithic integrated wavelength demultiplexer based on a waveguide rowland circle grating in InGaAsP/InP, J Lightwave Technol 16 (1998), 631–638.
8. D.A. Jackson, A.B. Lobo Riberio, L. Reeckie, and J.L. Archambault, Simple multiplexing scheme for a fiber-optic grating sensor network, Opt Lett 18 (1993), 1192–1194.
9. G.Z. Xiao, P. Zhao, F.G. Sun, Z.G. Lu, Z. Zhang, and C.P. Grover, Interrogating fiber Bragg grating sensors by thermally scanning an arrayed waveguide grating based demultiplexer, Opt Lett 29 (2004), 2222–2224.
10. Y. Sano and T. Yoshino, Fast optical wavelength interrogator employing arrayed waveguide grating for distributed fiber Bragg grating sensors, J Lightwave Technol 21 (2003), 132–139.
11. V.I. Tolstikhin, A. Densmore, K. Pimenov, Y. Logvin, F. Wu, S. Laframboise, and S. Grabtchak, Monolithically integrated optical channel monitor for DWDM transmission systems, J Lightwave Technol 22 (2004), 146–153.
12. Y.-J. Rao, Fiber Bragg grating sensors: Principles and applications, In: K.T.V. Grattan and B.T. Meggitt (Eds.), Optical fiber sensor technology, Vol. 2, Chapman & Hall, London, 1998, pp. 355–389.

A HYPERBOLIC SUMMATION METHOD TO FOCUS B-SCAN GROUND PENETRATING RADAR IMAGES: AN EXPERIMENTAL STUDY WITH A STEPPED FREQUENCY SYSTEM

Caner Ozdemir,[1] Sevket Demirci,[1] Enes Yigit,[1] and Adnan Kavak[2]
[1] Department of Electrical-Electronics Engineering, Mersin University, Ciftlikkoy, Mersin 33343, Turkey
[2] Department of Computer Engineering, Kocaeli University, Izmit, Kocaeli 41040, Turkey

Received 1 August 2006

ABSTRACT: *There are many techniques to focus raw B-scan ground penetrating radar (GPR) images mainly distorted from well-known hy-*